Seminar 53 – HVACR Novel Measurement Techniques: The Next Generation

Davide Ziviani, Ph.D.

Purdue University

dziviani@purdue.edu

Capacitive Void Fraction Sensors: Working Principle, Calibration, and Applications

Learning Objectives

- **Objective 1:** Explain high level operating principles of fiberoptic temperature measurement techniques
- **Objective 2:** Understand current used and new techniques to determine average and local air-side heat transfer coefficients
- **Objective 3:** Obtain an understanding of the different measurement methods that can be used for refrigerant and oil charge measurements
- **Objective 4:** Explain the relationship between the measured capacity and the void fraction

Acknowledgements

This research work is led by Prof. Michel De Paepe from Ghent University, Belgium. I would like to acknowledge Marijn Billiet for his instrumental help with the development of void fraction sensor for refrigerant-oil mixtures

Outline/Agenda

- Introduction
- Capacitance Sensor Construction
- Sensor Calibration
- Applications
  - Two-phase flow in hairpin tube in compact fin-and-tube HX
  - In-situ Oil Retention measurements (1721-RP)

Introduction

- The void fraction is an important parameter in many two-phase flow pressure drop and heat transfer correlations
- The void fraction is strongly related to the two-phase flow behavior, which strongly affects both total heat transfer rate and pressure drop
- A large variety of void fraction measurement techniques exist and each technique has some typical advantages and disadvantages:
  - Wire mesh tomography (Fuangworawong et al., 2007)
  - Hot wire anemometry (Louahlia-Gualous et al., 2003)
  - Optical techniques (Brutin et al., 2013)
  - Permittivity-based (Gijsenbergh and Pures, 2013)
- Capacitive void fraction methods (e.g., Strazza et al., 2011) are low cost and easy to implement. However, a drawback is that the relation between the void fraction and the measured capacitance has to be determined for each design and application
- In order to make the measurement technique more widely applicable, the calibration has to be independent of variables other than those measured with the sensor itself.
- De Kerpel et al., 2013 proposed to correlate void fraction and flow regime based on the capacitance signal alone

Capacitance Sensor Construction

- The sensor consists of two main parts: the sensor probe and the sensor transducer (Carnier, 2009)
- The probe contains the sensing and guard electrodes and is built into the test section
- The sensor transducer comprises the electronics necessary to measure the capacitance between the sensing electrodes of the probe.
- The concave electrodes are placed around the tube wall with $\beta = 160°$
- To attain a high sensitivity to the capacitance changes of the two-phase flow, the thickness of the tube wall should be small
- A flexible circuit material is used to maintain a thin tube wall. The material is a laminate of a thin layer of dielectric material and a layer of copper cladding, The electrodes are etched from the copper claddings and the dielectric layer acts as the tube wall with a thickness of 50 μm
- Axial length of the electrodes is 8 mm (0.315 in)

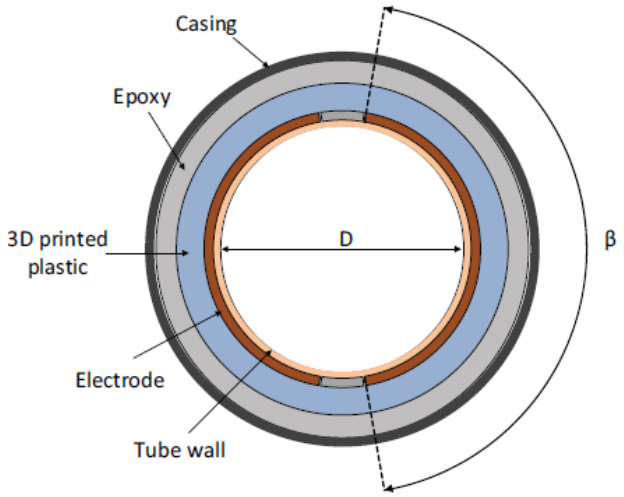

Cross-section of the sensor as designed by Carnier, 2009.

Capacitance Sensor Construction (cont'd)

- The sensor probe contains three electrode pairs:
  - The middle electrodes are the sensing electrodes, between which the capacitance is measured
  - The two outer electrodes act as guard electrodes to reduce the fringing of the electric flied lines
- 3D printed plastic parts are used to give structural integrity to the tube wall and electrodes and a smooth transition is ensured
- The assembly is placed in an aluminum casing which will act as a shield for the electromagnetic interference
- The gaps between the plastic parts and the casing are filled with a two-component epoxy potting compound
- The sensor transducer is connected to the sensor probe to measure the capacitance between the sensing electrodes of the probe
- The transducer circuit is based on the design of a stray-immune capacitance meter (Yang and Yang, 2002). Without stray-immunity is difficult to measure small capacitances of e.g., < 10pF
- Output of the transducer is 0 to 10 V with a sensitivity of 1.16 V/pF and output accuracy of 4 mV (at 1kHz)

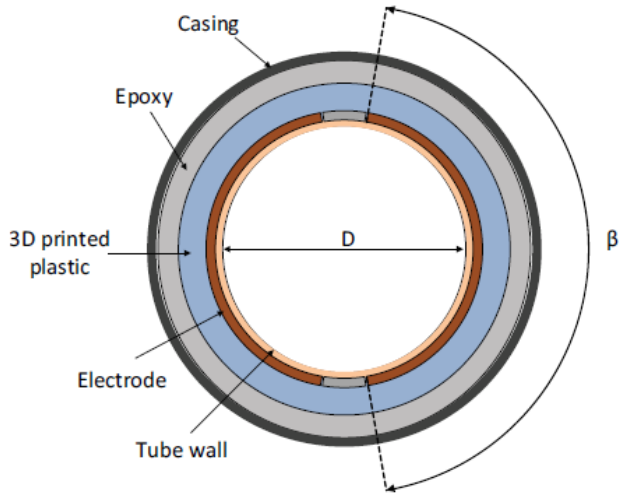

Cross-section of the sensor as designed by Carnier, 2009.

Sensor Calibration

- Due to the difference between dielectric constant of the gas and liquid phase, the measured capacitance between the electrodes depends on the void fraction (**C-ε**)
- Due to the curvature of the electrodes, the electric field is not homogeneous
- The measured capacitance is dependent on the void fraction as well as the spatial distribution of the phases (the capacitance does not linearly vary with the void fraction)

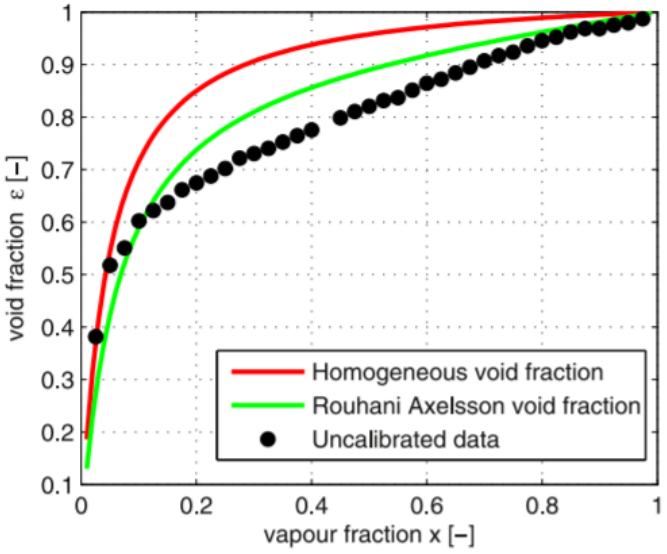

Example: void fraction measured with uncalibrated sensor (linear C-ε relation assumed) for R410A, $T = 15°\mathrm{C}$ (59 °F) and $D = 8\ \mathrm{mm}\ (0.315\ \mathrm{in})$ for $G = 200\ \mathrm{kg/m^2}$ ($40.96\ \mathrm{lb/ft^2 s}$) (De Kerpel et al., 2013)

Steiner version of Rouhani-Axelsson drift flux void fraction model was chosen as high accuracy model:

$$\varepsilon = \frac{x}{\rho_v}\left[\left(1 + 0.12(1-x)\left(\frac{x}{\rho_v} + \frac{1-x}{\rho_l}\right) + \frac{1.18(1-x)\left(g\sigma(\rho_l - \rho_v)\right)^{0.25}}{G\rho_l^{0.5}}\right)\right]^{-1}$$

Homogeneous void fraction model is also shown as an indication of the upper limit of the actual void fraction

- Calibration of the void fraction sensor is necessary

Sensor Calibration (cont'd)

- C-ε curves depends on the flow regime
- Simplified flow structures are assumed for each flow regime based on geometric models proposed by Thome and coworkers (De Kerpel et al., 2013)
- FEM simulations are used to determine the C-ε relation for each of these liquid-vapor interface structures (flow regimes). FEM is utilized due to relatively complex liquid-vapor interfaces and avoids the use of inserts to mimic the vapor and liquid phase in the sensor

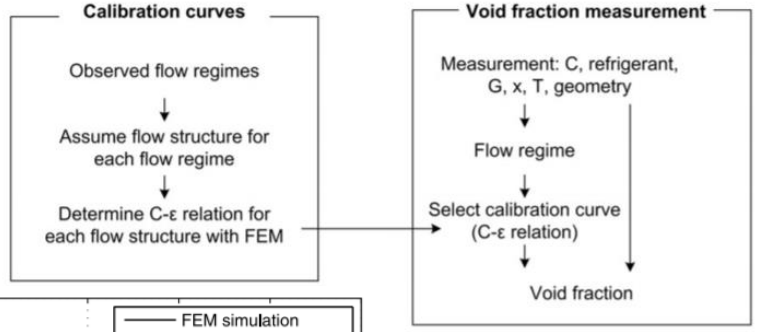

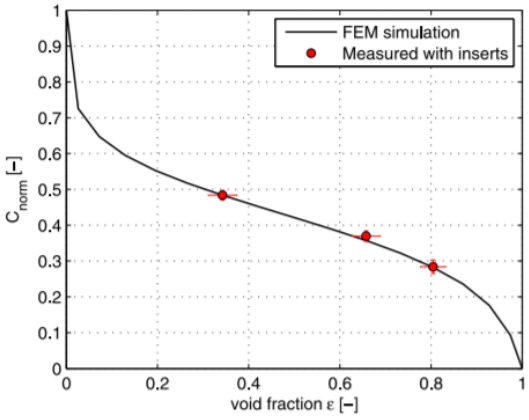

Comparison of the capacitances measured for the inserts and the ones predicted by the FEM simulation

$$C_{\text{norm}} = \frac{C_{\text{meas}} - C_{\text{vap}}}{C_{\text{liquid}} - C_{\text{vap}}}$$

Dielectric constant of the liquid phase and the vapor phase at ambient temperature

Refrigerant	chemical name	k_L [-]	k_V [-]
R11	Trichlorofluoromethane	1.92	1.009
R22	Chlorodifluoromethane	6.12	1.004
R32	Difluoromethane	14.27	1.0102
R134a	1,1,1,2-tetrafluoroethane	9.51	1.0125
R245fa	1,1,1,3,3,-pentafluoropropane	6.82	1.0066
R290	Propane	1.27	1.009

Effect of layer of plastic around the electrodes on the measured capacitance

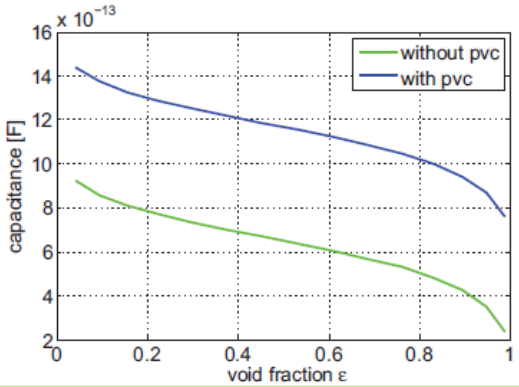

Sensor Calibration (cont'd)

- Two-flow maps:
  1. Wojtan-Ursenbacher-Thome (Wojtan et al., 2005) flow map
  2. Intermittent-annular transition boundary by Barbieri et al. (2008) combined with the slug-intermittent transition boundary of the Wojtan-Ursenbacher-Thome flow map

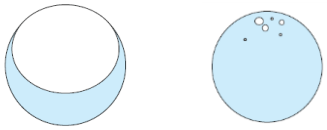

Schematic representation of the interface structures for slug flow: large vapor bubble; liquid slug

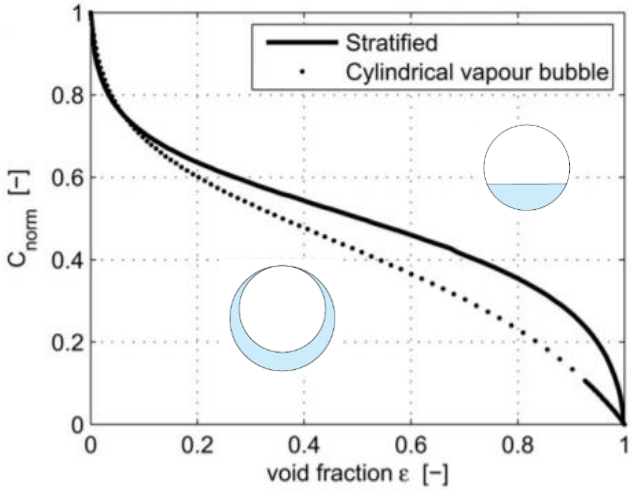

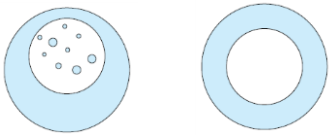

Schematic representation of the annular flow structure and the simplified interface structures

Entrained liquid fraction in the vapor core is determined with the correlation from Oliemans et al.,

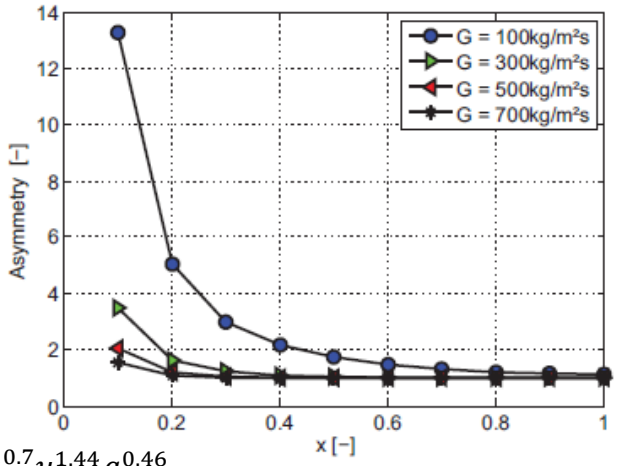

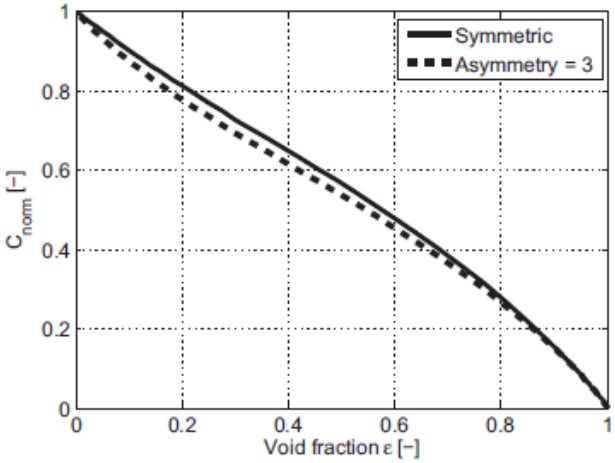

$$\frac{e}{1-e} = 10^{-2.52}\rho_l^{1.08}\rho_v^{0.18}\mu_l^{0.27}\mu_v^{0.28}\sigma^{-1.8}d_h^{1.72}u_{sl}^{0.7}u_{sv}^{1.44}g^{0.46}$$

Sensor Calibration (cont'd)

- Calibration results for R134a, the weighting for intermittent flow is given by:

$$\varepsilon_{\text{intermittent}} = \frac{(1-F95)\mu\sigma\varepsilon_{slug} + (1-\mu)(1-\sigma)F95\varepsilon_{\text{annular}}}{(1-F95)\mu\sigma + (1-\mu)(1-\sigma)F95}$$

- The flow regimes are assigned based on the flow regime map by Wojtan et al. Two void fraction models are shown for reference the Steiner version of the Rouhani-Axelsson model and the homogenous void fraction

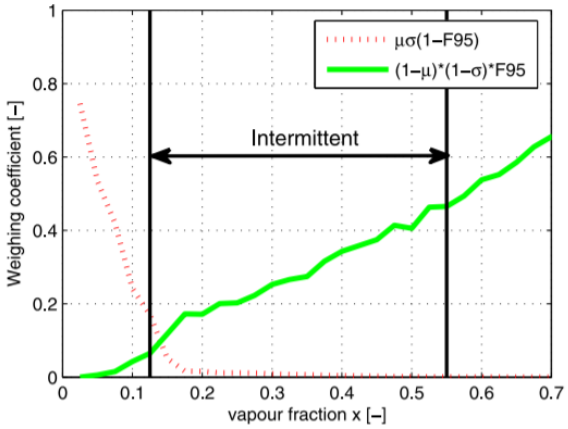

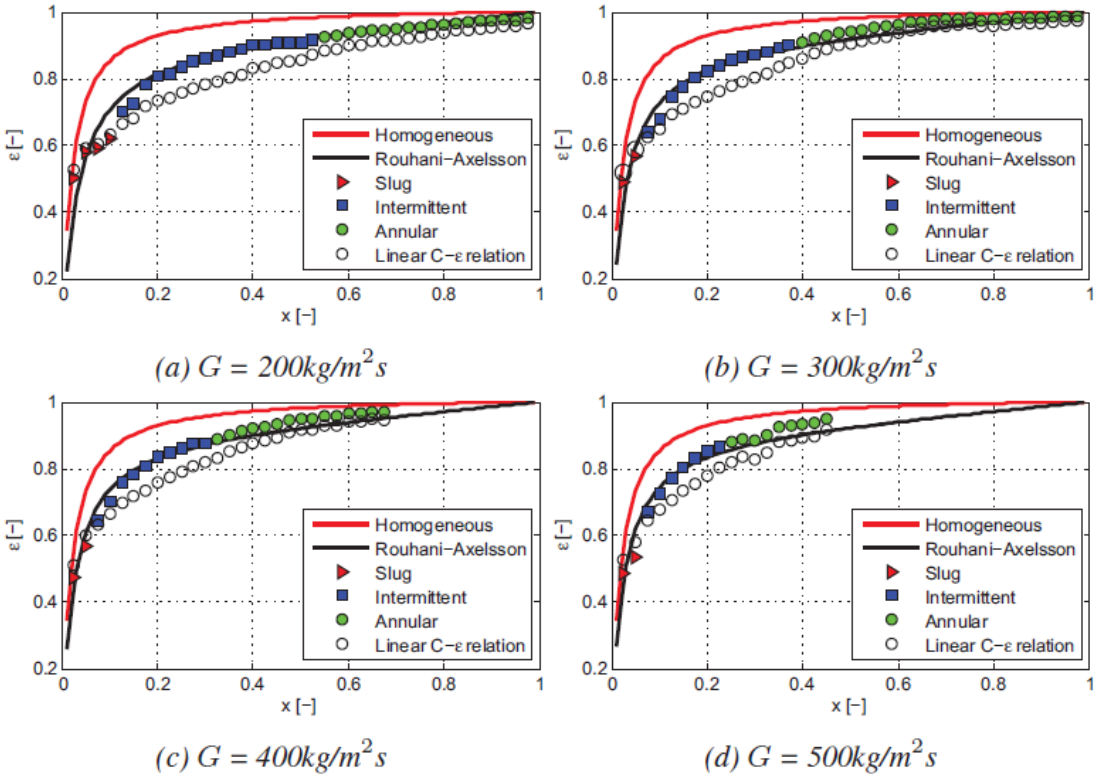

(a) $G = 200 kg/m^2 s$ (b) $G = 300 kg/m^2 s$

(c) $G = 400 kg/m^2 s$ (d) $G = 500 kg/m^2 s$

$1\ \text{kg/m}^2\text{s} = 0.2048\ \text{lb/ft}^2\text{s}$

Sensor Calibration (cont'd)

Normalized sensor signal for different G and x for R410A: (a) slug flow and intermittent flow at low x; (b) intermittent flow at high x and annular flow

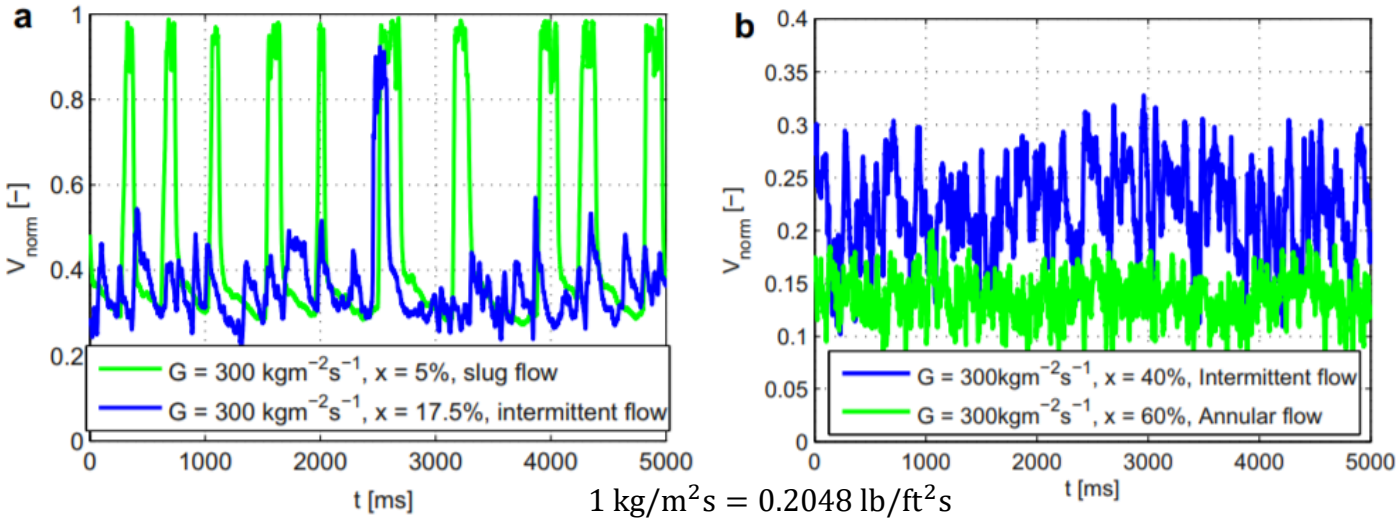

$1\ \mathrm{kg/m^2s} = 0.2048\ \mathrm{lb/ft^2s}$

	Statistical parameters		Flow regime map				Linear $C-\varepsilon$ relation	
			Thome flowmap		Barbieri flowmap			
	AVG (%)	STD (%)	AVG (%)	STD (%)	AVG (%)	STD (%)	AVG (%)	STD (%)
R410A, slug flow	6.6747	10.5223	1.7492	10.68	1.7492	10.68	18.43	17.81
R410A, intermittent flow	0.6271	2.9341	2.0793	3.5878	2.0824	4.3032	−7.33	2.77
R410A, annular flow	0.8289	1.2802	0.2731	1.6120	0.5477	1.4775	−2.56	2.45
R410A, total	1.2749	4.0689	1.0652	4.6661	1.1539	4.7400	−2.6	9.07
R134a, slug flow	0.0695	11.6995	−3.6619	9.3178	−3.6619	9.3178	5.03	12.86
R134a, intermittent flow	−0.6328	1.6172	0.4864	1.8933	−0.297	1.2539	−8.17	1.63
R134a, annular flow	1.3751	1.6030	1.218	1.5783	1.3919	1.4756	−2.02	1.66
R134a, total	0.5017	3.6574	0.1529	4.4432	0.1171	4.397	−4.04	5.44

Applications: Return Bend Two-Phase Pressure Drops

- Compact heat exchangers for domestic use
- Objectively assess the intensity and extent of the disturbance of the two-phase flow behavior and pressure drop due to a return bend
- Link flow behavior to the pressure drop

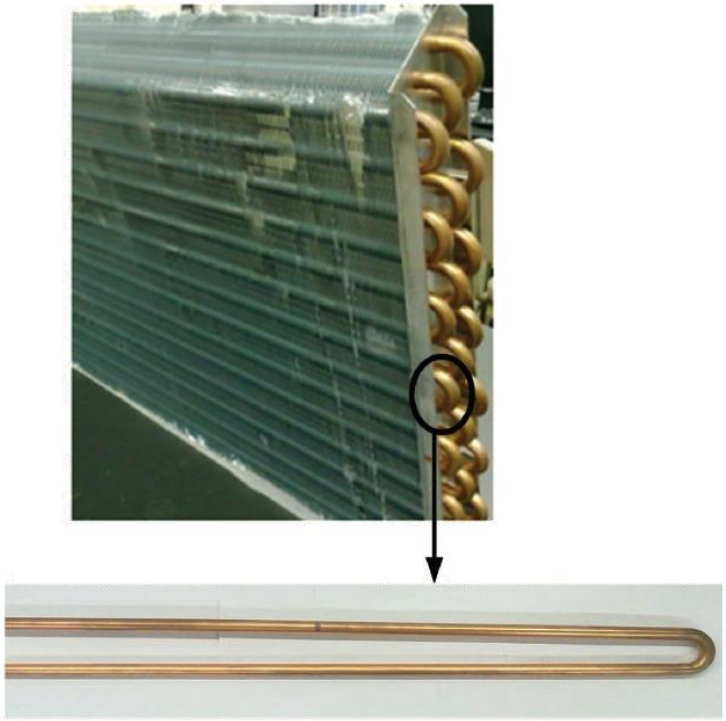

	OD (mm)	*ID* (mm)	*R* (mm)	2*R*/*ID* (–)
Geometry 1	9.53	8.1	10.2	2.55
Geometry 2	9.53	8.1	12.7	3.13
Geometry 3	9.53	8.1	16	3.95
Geometry 4	6.35	4.93	10.9	4.43

$1\ \text{mm} = 0.0394\ \text{in}$

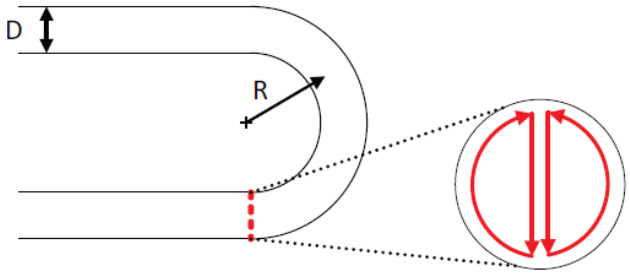

Applications: Return Bend Pressure Drops (cont'd)

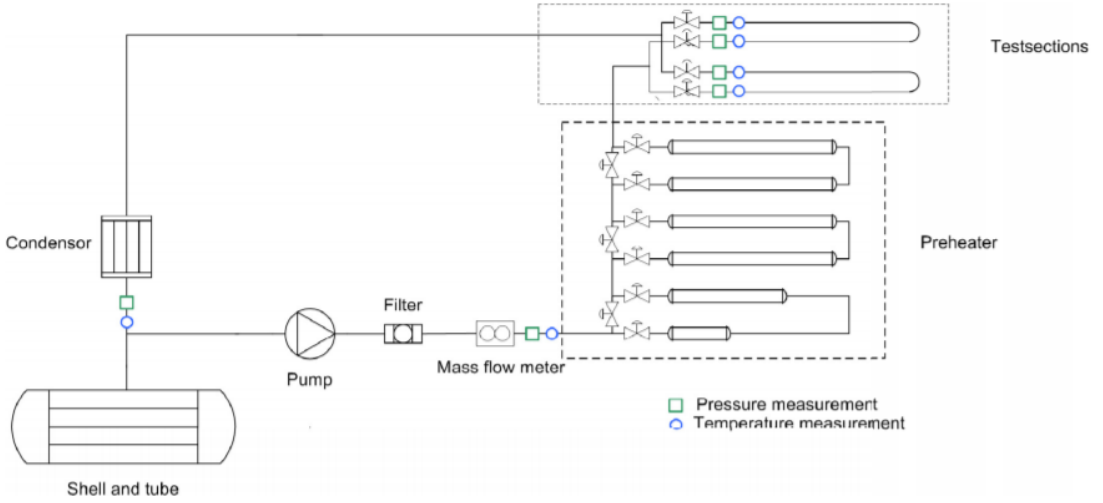

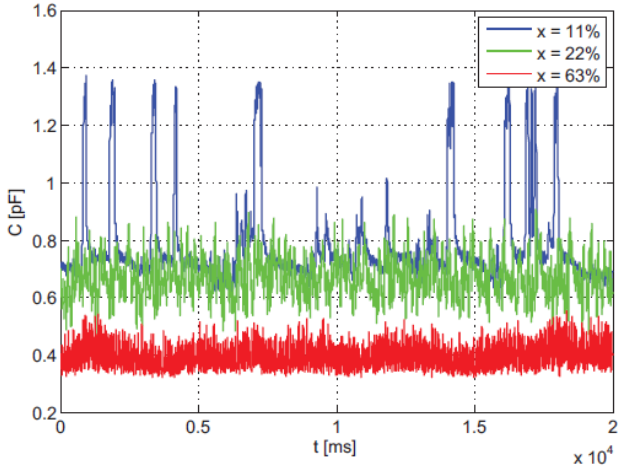

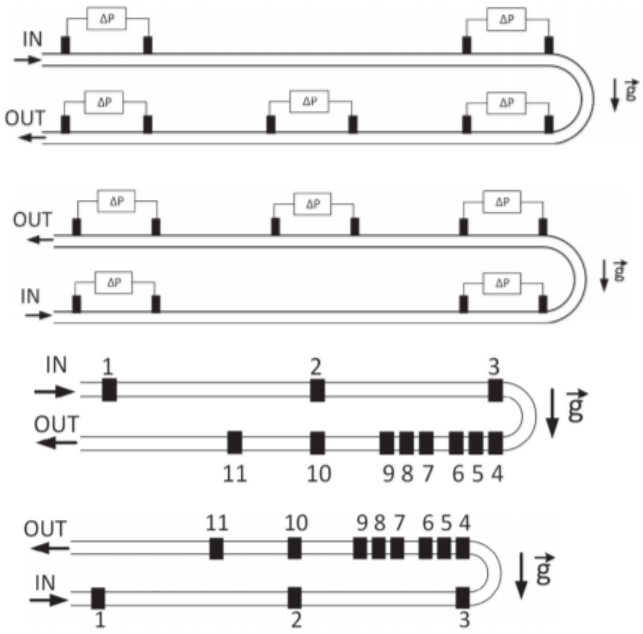

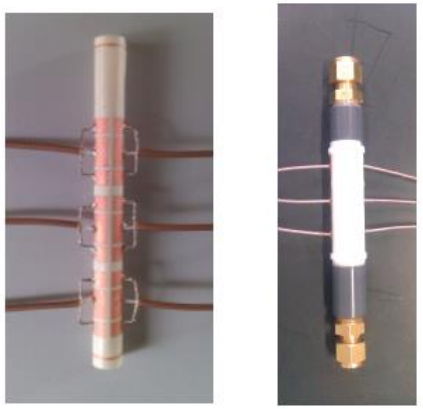

Capacitance time trace for R134a, $T = 15°\text{C}$ (59 °F) and $D = 8$ mm (0.315 in) for $G = 300\ \text{kg/m}^2$ (61.45 $\text{lb/ft}^2\text{s}$) at different vapor qualities

Applications: Return Bend Pressure Drops (cont'd)

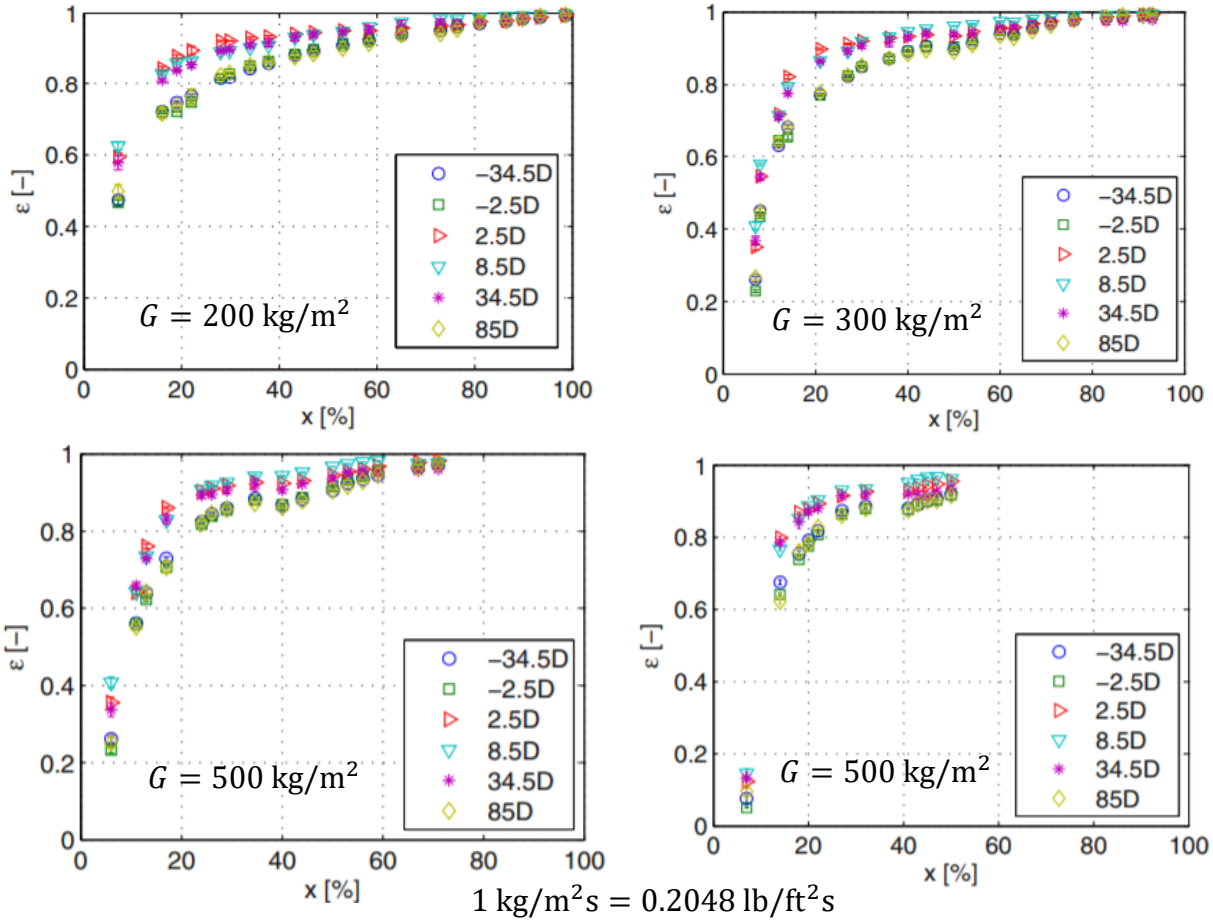

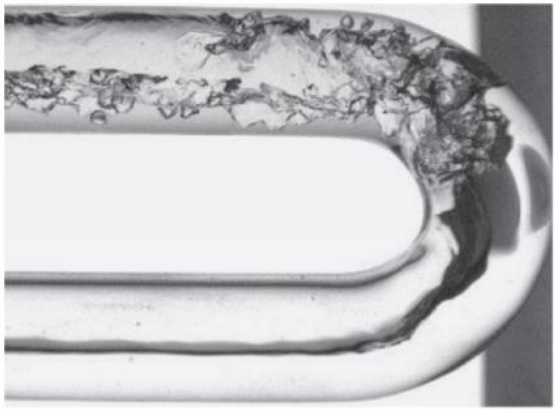

$1\ \mathrm{kg/m^2 s} = 0.2048\ \mathrm{lb/ft^2 s}$

Average flow behavior: time-averaged void fraction for downward oriented flow at different locations up- and downstream of the return bend for R134a

Applications: Return Bend Pressure Drops (cont'd)

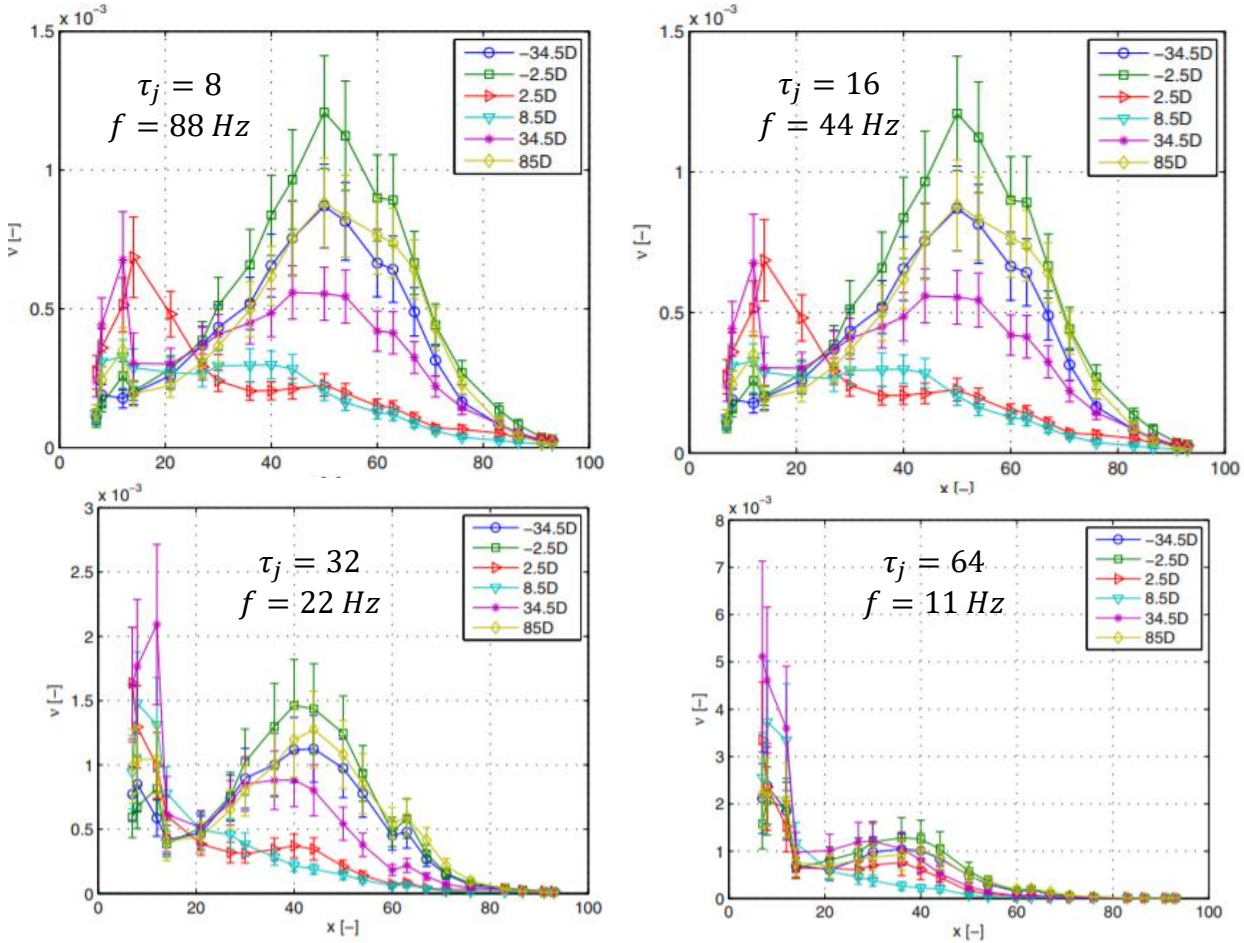

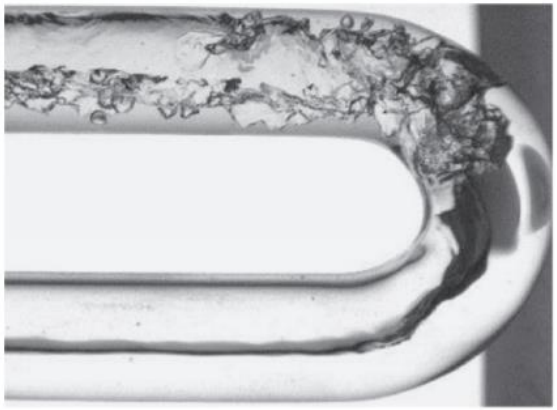

Dynamic component based on wavelet variance analysis of the signal: wavelet variance for downward oriented flow at several scales (frequencies) for $G = 300\ \mathrm{kg/m^2}$ (61.45 $\mathrm{lb/ft^2 s}$)

Applications: In-situ Oil Retention Measurements (cont'd)

- 1721-RP: Oil Return and Retention in Unitary Split System Gas Lines with HFC and HFO Refrigerants

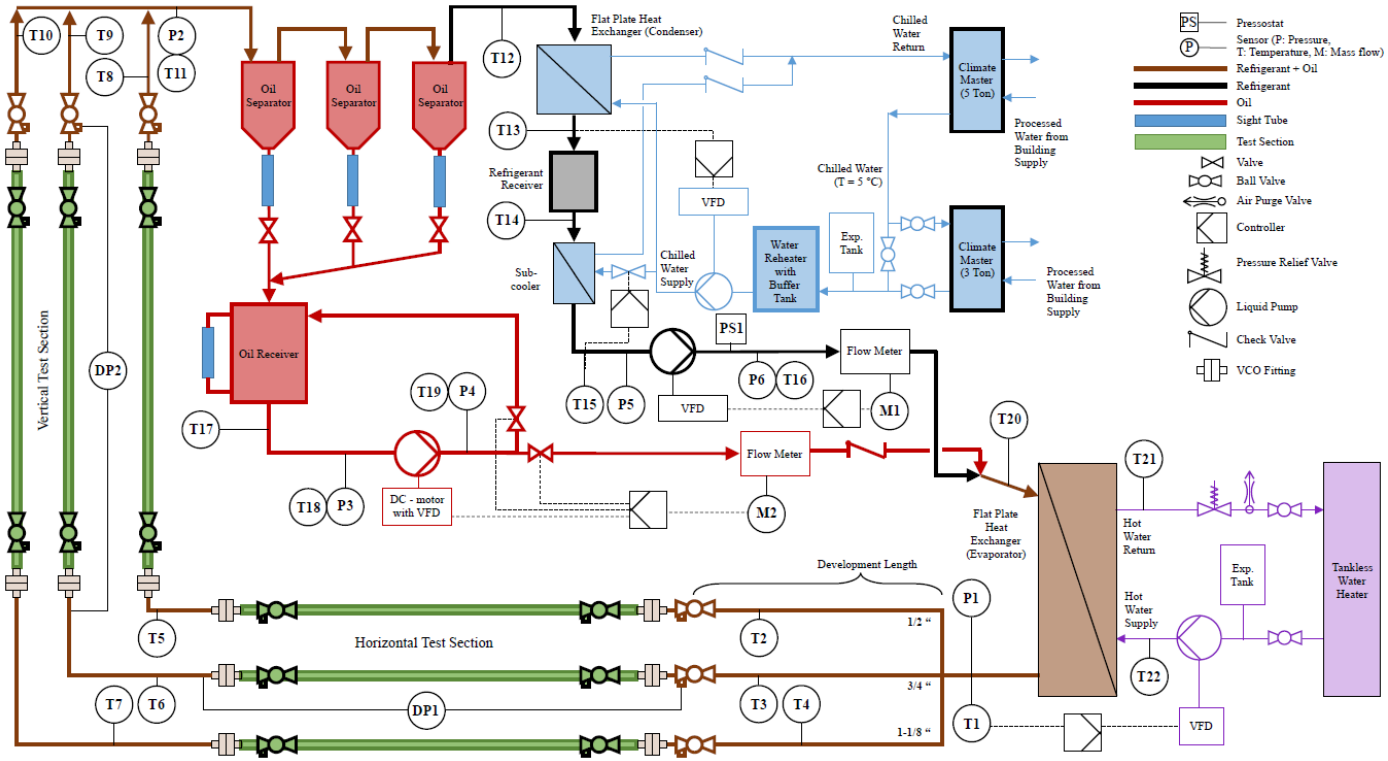

Applications: In-situ Oil Retention Measurements (cont'd)

- 1721-RP: Oil Return and Retention in Unitary Split System Gas Lines with HFC and HFO Refrigerants

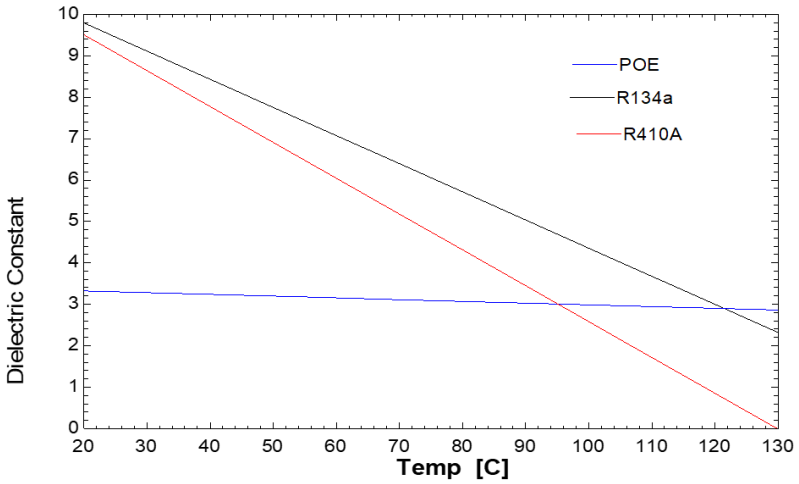

(68 °F to 266 °F)
From Fukuta et al. (1999)

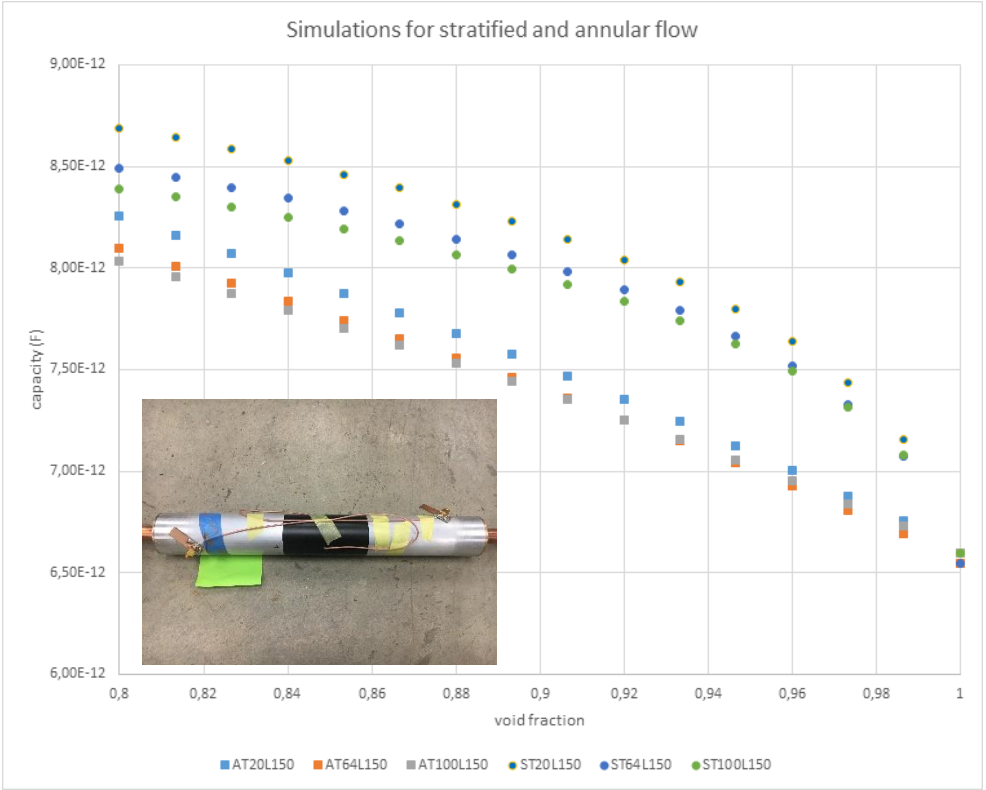

Simulations for R134a and POE32
(standard deviation of electronics ± 0.012 pF)

Conclusion

- Electrical capacitance of the flow is an effective way of assess the flow behavior
- The capacitance of a fluid is a direct function of the amount of each phase
- A sensor has been developed to measure the void fraction based on the capacitance of the flow
- A calibration technique based on signal features has been proposed and validated. This was achieved by using three statistical parameters of the capacitance signal to determine the flow regime and as weighting coefficients to determine the void fraction for intermittent flows:
  - mean capacitance
  - the variance of the capacitance signal
  - the frequency for which 95% of the frequency spectrum of capacitance signal is lower
- The applicability of this methodology can be extended to different flow regimes and refrigerant-oil mixtures
- The capacitance sensor have been employed to investigate the effect of bend geometry on the two-phase frictional pressure drop and flow behavior in the vicinity of the bend
- The ongoing research is developing a void fraction sensor for measuring instantaneous and average oil-circulation ratios in horizontal and vertical lines

Bibliography

- Barbieri, P.E.L., Jabardo, J.M.S., Bandarra Filho, E.P., 2008. Flow Patterns in Convective Boiling of R-134a in Smooth Tubes of Several Diameters. Fifth European Thermal-Science Conference, The Netherlands.
- Carniere, H., Bauwens, B., T'Joen, C., De Paepe, M., 2009. Probabilistic mapping of adiabatic horizontal two-phase flow by capacitance signal feature clustering. *International Journal of Multiphase Flow*, 35, 650-660.
- De Kerpel, K., Armeel, B., T'Joen, C., Carniere, H., De Paepe, M., 2013. Flow regime based calibration of a capacitive void fraction sensor for small diameter tubes. *International Journal of Refrigeration*, 36, 390-401.
- De Kerpel, K., Armeel, B., De Schampheleire, S., T'Joen, C., Carniere, H., De Paepe, M., 2014. Calibration of a capacitive void fraction sensor for small diameter tubes based on capacitive signal features. *Applied Thermal Engineering*, 63, 77-83.
- De Kerpel, K., De Schampheleire, S., De Keulenaer, T., De Paepe, M., 2016. Effect of the bend geometry on the two-phase frictional pressure drop and flow behaviour in the vicinity of the bend. *Applied Thermal Engineering*, 104, 403-413.
- Fukuta, M., Yanagisawa, T., Ogi, Y., Tanaka, J., 1999. Measurement of Concentration of Refrigerant in Refrigeration Oil by Capacitance Sensor. Trans. Of the JSRAE, 16, 239-248.

Bibliography (cont'd)

- Gijsenbergh, P., Pures, R., 2013. Permittivity-based void fraction sensing for microfluidics. *Sensor and Actuators A: Physical*, 195, 64-70.
- Oliemans, R.V.A., Pots, B.F.M., Trompe, N., 1986. Modelling of annular dispersed two-phase flow in vertical pipes. *International Journal of Multiphase Flow, 12, 711-732.*
- Yang, S.X., Yang, W.Q., 2002. A portable stray-immune capacitance meter. *Rev. Sci. Instrum.*, 73, 1958-1961.
- Wojtan, L., Ursenbacher, T., Thome, J.R., 2005. Measurement of dynamic void fractions in stratified types of flow. *Exp. Therm. Fluid Sci.*, 29, 383-392.

Questions?

Davide Ziviani

dziviani@purdue.edu